

International Journal of Innovative Technology and Interdisciplinary Sciences

https://journals.tultech.eu/index.php/ijitis ISSN: 2613-7305 Volume 8, Issue 4



DOI: https://doi.org/10.15157/IJITIS.2025.8.4.970-993 Received: 26.08.2025; Revised: 21.10.2025; Accepted: 01.11.2025

Research Article

Modelling Transient Hydraulic Hammer Behavior in Pumped Systems Using WHAMO Software

Gjelosh Vataj^{1*}, Meshdi Ismayilov², Zenel Sejfijaj^{3*}, Erdeta Vataj⁴

- ¹ Faculty of Engineering and Informatics, The University of Applied Science in Ferizaj (UASF), Kosovo.
- ² Faculty of International Relation and Economics Baku, State University, Azerbaijan
- ³ The Independent Commission for Mines and Minerals, 10000 Prishtina, Kosovo
- ⁴ Faculty of Architecture, University of Prishtina "Hasan Prishtina", 10000 Prishtina, Kosovo.
- *gjelosh.vataj@ushaf.net, zsejfijaj@hotmail.com

Abstract

This paper presents a mathematical model of the hydraulic hammer phenomenon. The model incorporates the momentum and continuity equations, the construction of the system layout, and the junctions within the pipeline network. Potential scenarios during system operation are analyzed using the Water Hammer and Mass Oscillation (WHAMO) software to simulate transient hydraulic behavior. In closed hydraulic systems, a hydraulic hammer occurs when the system transitions from a stable to an unstable state, causing the kinetic energy of the fluid to be rapidly converted into pressure energy. This results in a powerful pressure surge accompanied by a reverse flow wave. Such pressure fluctuations can lead to extremely low pressures, increasing the risk of contaminant intrusion through cracks or pipe damage. This phenomenon often accompanied by a hammer-like sound poses a significant challenge in drinking water treatment systems. Because the governing equations are nonlinear and hyperbolic, analytical solutions are not feasible; therefore, numerical modeling is required. The main goal of this study is to analyze pump behavior during transient conditions associated with the water hammer phenomenon.

Keywords: Hydraulic Hammer Phenomenon; Closed Hydraulic Systems; Node; WHAMO Software.

INTRODUCTION

Hydraulic transients are unsteady flow phenomena that occur in pressurized pipe systems due to sudden changes in velocity or pressure [1]. Among these, the hydraulic hammer commonly known as water hammer is one of the most significant, as it can cause severe mechanical and operational impacts on hydraulic networks.

In this research work, the hydraulic hammer phenomenon is simulated using the WHAMO software to evaluate potential scenarios that may occur during system interventions [2]. In closed hydraulic systems, such as the one analyzed in this study, hydraulic hammer typically arises when the system transitions from a stable to an unstable state, causing the kinetic energy of the moving fluid to be abruptly converted into pressure energy. The term "hydraulic hammer" originates from the distinctive hammer-like sound produced during this event.

International Journal of Innovative Technology and Interdisciplinary Sciences



https://doi.org/10.15157/IJITIS.2025.8.4.970-993

© 2024 Authors. This is an Open Access article distributed under the terms and conditions of the Creative Commons Attribution 4.0 International License CC BY 4.0 (http://creativecommons.org/licenses/by/4.0).

Alongside the high-pressure wave, a counter-current wave is also generated, which is often overlooked but can result in extremely low pressures. These low-pressure zones may allow contaminants to enter the fluid through cracks or damaged sections of the pipeline [3]. Water hammer represents a common yet critical issue in drinking water treatment systems, as it can induce additional stress on pipes, joints, and other components, potentially compromising system performance and safety.

The governing momentum and continuity equations form a set of nonlinear, hyperbolic differential equations that cannot be solved analytically. Due to the complexity of the phenomenon and the numerous parameters involved, specialized modeling software is required to achieve accurate numerical solutions [4]. This paper presents a numerical investigation of the transient behavior of pumps in closed hydraulic systems during the occurrence of the hydraulic hammer phenomenon. Additionally, the specific objectives of this research are as follows:

- To study the hydraulic, energy, and economic indicators associated with fluid flow problems in hydraulic water networks, with the fundamental goal of identifying the optimal scenario for managing water hammer.
- To develop a theoretical mathematical model of an industrial water transport system.
- To determine and analyze the key parameters influencing the occurrence and intensity of the hydraulic hammer phenomenon.
- To perform both steady-state and unsteady-state analyses of the industrial water transport model using WHAMO software.
- To investigate the factors contributing to abnormal pump operation during transient conditions.
- To propose possible intervention scenarios during the water hammer process aimed at mitigating or eliminating its negative consequences.

CASE STUDY: HYDRAULIC SYSTEM STARTING AT NODE 0 (ELEVATION 544.53 m above sea level).

Figure 1 illustrates the system that serves as the object of study in this paper, along with a description of the system in terms of nodes and pipe data. The system starts at node 0, a water intake points 544.53 m a.s.l. The length of the pipe from the water intake to the pumping station in Miloshevo is 8941.17 m, while from the pumping station in Miloshevo to the water treatment plant "Shkabaj" is 4523.88 m. The entire length of the DN1200 pipe DCI from the intake point to the water treatment plant in Shkabaj is 13465.05 m.

The level difference between node 0, the water intake site, and the pumping station, node 17, is 11.56 m, while the level difference between the pumping station, node 18, and the water treatment plant, node 28 is 65.26 m

In 2023, the parameters of the Johnson-Cook and GISSMO damage models were developed and optimized using advanced finite element methods (FEM) to predict the

failure behavior of dual-phase steels (DP600 and DP800) [5]. The numerical simulations showed strong agreement with experimental test results, confirming the effectiveness of the combined modeling approach in accurately simulating damage initiation and fracture progression in advanced structural materials [6].

The entire water treatment system of the SHKABAJ factory is designed to operate in two phases [7].

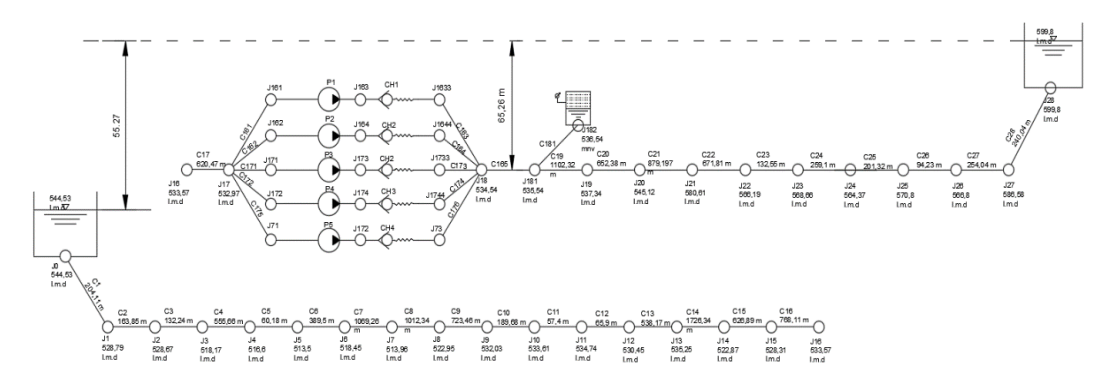


Figure 1. System diagram [7].

The first phase produces drinking water with a production capacity of $Q = 321 \div$ 770 l/s.

The second phase will produce drinking water with the factory's production capacity $Q = 573 l/s \div 1375 l/s$. of:

Additionally, the water hammer phenomenon is analyzed using WHAMO 3.0 software, based on the pump flow conditions presented in the preceding section.

The technical characteristics of the pumps are:

•	Flow	Q = 343.00 l/s,
•	Geodetic height	H = 84 m,
•	Media	Water 100%,
•	Density	$\rho = 998.20 kg/m^3$
•	Neto positive section head NPSH	6.01 <i>m</i> ,
•	No. of pump rotations	n = 1485 rpm

The information received on 18.12.2019 for the Miloshevo station and the Shkabaj plant is as follows:

- The minimum inlet pressure has the value of 11.4 m.
- The maximum inlet pressure has a value of 18 m.
- The minimum outlet pressure has a value of 94.9 m.
- The maximum outlet pressure has the value of 97.6 m.

The statements above and accompanied with chart characteristics of the pumps operating are shown in the Figure 2.

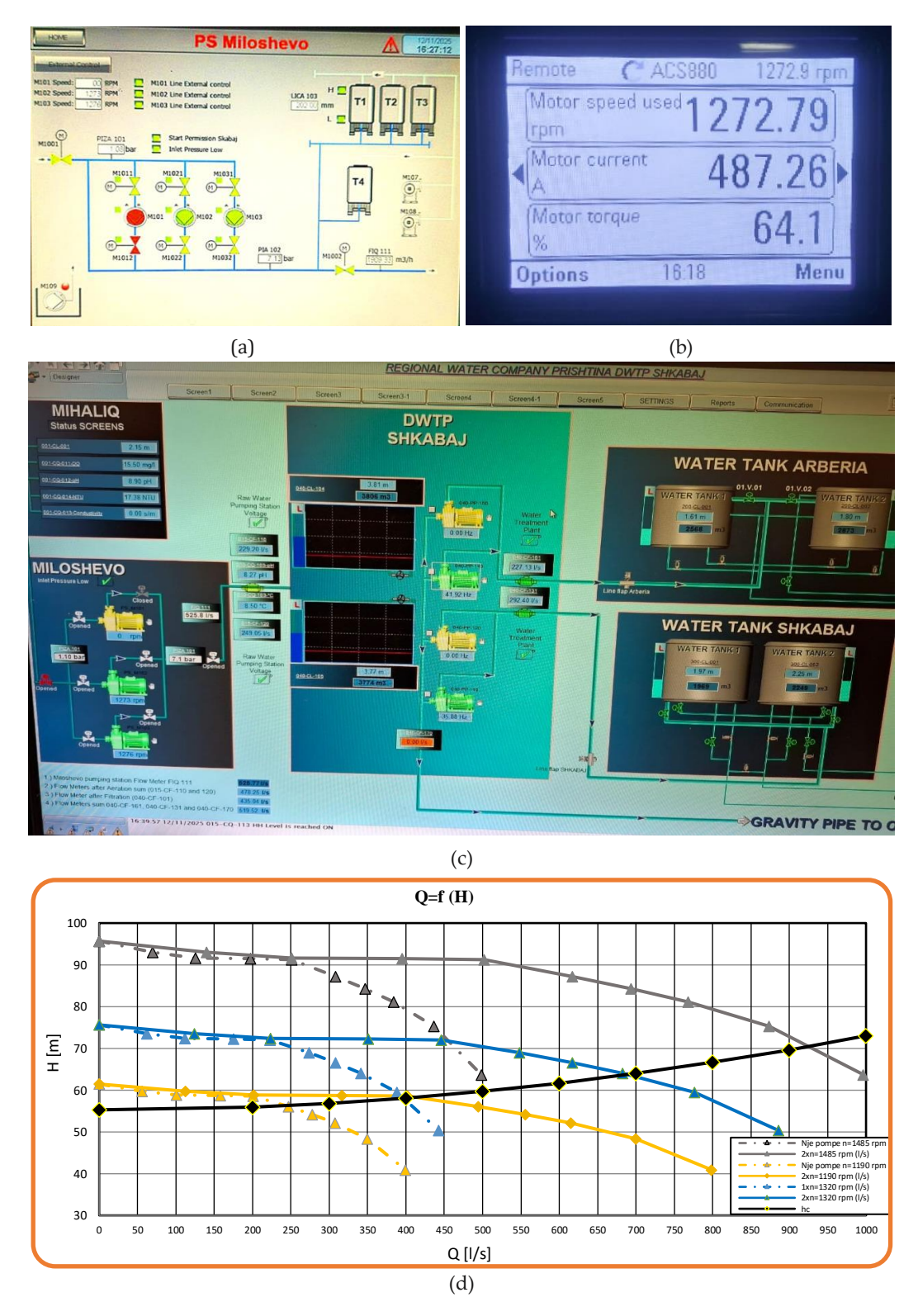


Figure 2. Characteristics of pumps operating alone and in parallel concerning *rpm*. (a)- Photo of the SCADA system screen PS Miloshevo, (b)- Photo of the Variable Frequency Drive (VFD), (c)- Photo of the SCADA system screen (d)- Chart characteristics of the pumps operating

In Figure 2, we present the characteristics of the pumps when operating with a single pump and when two pumps are running in parallel at different motor speeds of 1190 rpm, 1320 rpm, and a maximum motor speed of 1485 rpm.

Furthermore, Table 1 contains essential information regarding this data. Table 2 depict the comparison of flow and geodetic height of pumps.

A pump n=1485 rpm Q1+Q2 A pump n=1320 rpm Q1+Q2 Q1+Q2 A pump n=1190 rpm WILO (1 pump) 1485 WILO (1 pump) WILO (1 pump) 1190 1320 rpm rpm rpm O Н Р M (1/s)O Н P Μ o Н P Μ (1/s)(1/s)(1/s)(m) (kW) (Nm) (1/s)(m) (kW) (Nm) 1/s(m) (kW) (Nm) 0.0 138.6 95.7 197.4 1,270.0 0.0 0.0 75.6 1,003.4 0.0 0.0 61.4 101.5 815.5 0.0 70.1 93.0 203.1 1,306.7 140.2 62.3 73.4 142.6 1,032.4 124.6 59.7 104.5 839.1 112.3 56.1 251.4 72.3 157.8 1257 91.6 224.8 1,446.3 111.7 1.142.7 223 4 100.7 58.8 115.6 928.7 2014 265.8 1,710.0 395.2 1976 915 1756 72.3 1866 1.351.1 351.2 158.3 58.7 1.098 1 3166 1367 250.9 301.4 1,939.1 501.8 223.0 72.0 211.6 1,532.1 446.0 201.0 58.5 155.1 1.245.2 402.1 308.5 87.2 328.8 2,115.4 617.0 274.2 230.9 1,358.4 68.9 1.671.4 548.4 247.2 56.0 169.2 494.4 351.1 2,258.8 694.0 278.0 1,450.5 347 0 84 3 308 4 246.5 1,784.8 6168 54 1 1806 556 1 66.6 367.0 2,361.1 768.0 1,865.6 682.6 307.7 384.0 341.3 64.0 257.7 52.0 188.8 1.516.2 615.4 436.7 75.3 391.4 2,518.1 873.4 388.1 59.5 274.8 1,989.6 776.3 349.9 48.3 201.4 1,617.0 699.9 399.3 40.9 212.5 1,706.3 498.3 63.7 413.0 2.657.1 996.6 442.9 50.3 290.0 2.099.4 885.8 798.6

Table 1. Characteristics of pumps depending on the number of revolutions

Table 2. Comparison of flow and geodetic height of pumps

Q	0	200	300	400	500	600	700	800	900	1000	1100
Hc	55.27	55.98	56.86	58.11	59.71	61.66	63.97	66.63	69.65	73.03	76.75

SELECTED SCENARIO: DUAL PUMP OPERATION WITH CLOSED SECTOR VALVE

In this scenario, the pumps operate at a speed of n=1320 rpm with a total flow rate of 700 l/s. The water transport system runs continuously until the 6th second, when the valve of sector V1, located at node J28, is closed, see Figure 3.

The pump station is equipped with an expansion tank, and the pumps maintain a flow rate of approximately 700 l/s, also at a rotation speed of 1320 rpm. The pumps are stopped after 25 seconds. Water is sourced from the village of Mihaliq and is transported by gravity to the pump station in Miloshevo. The pumps convey water through a 1200 mm pipe to the SHKABAJ factory reservoir.

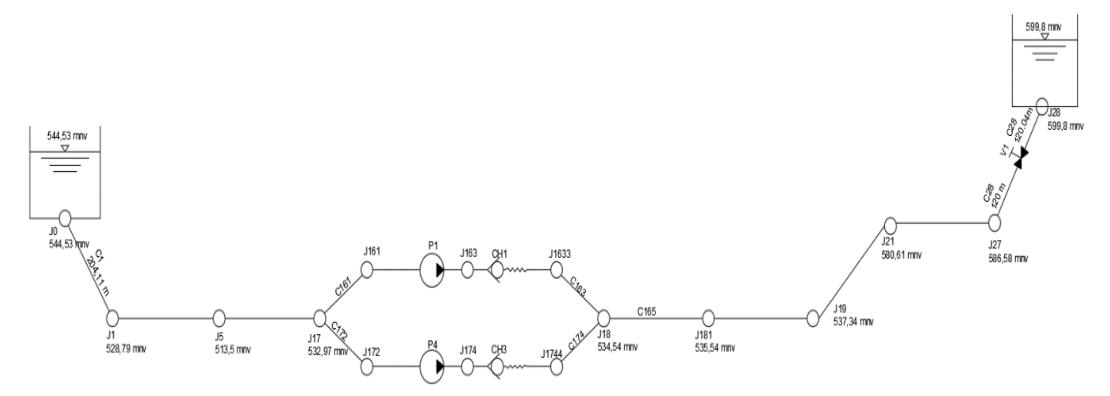


Figure 3. System diagram, scenario

Furthermore, the input parameters for the first simulation are summarized in Table 3.

Friction Geodetic Pump Number of Pipe Closing Speed Producer elevation flow v(m/s)losses Rotations of the diameter time of V1 of Pumps H (m) Q(l/s)(m) pump (rpm) (mm) t (s) 700 0.028 1200 84.00 1.219 1320 WILO

Table 3. Input parameters for this scenario

The water transport system outlined in Figure 4 operates by taking water from an altitude of 544.53 m above sea level.

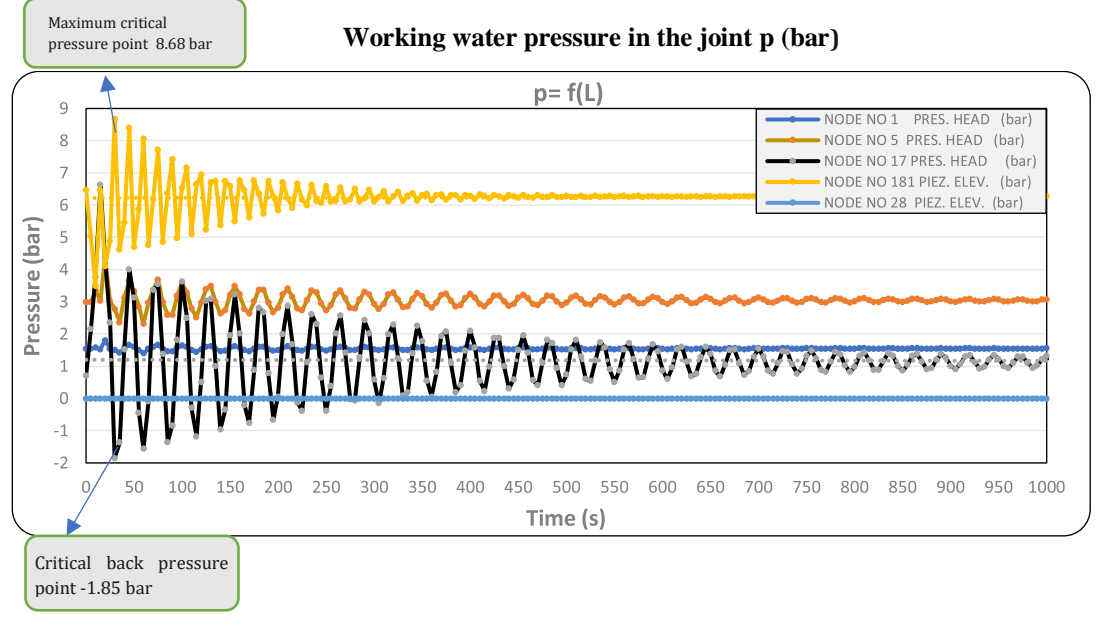


Figure 4. Comparison of water pressure at joints in the main pipe, without expansion vessel with number of rotations n=1320 rpm.

The water is conveyed by gravity through a ductile cast iron (DCI) pipeline with a diameter of 1200 mm (DN 1200) and a pressure rating of 12 bar (PN12) over a total length of approximately 9.5 km, reaching the "Miloshevë" Pump Station situated at an elevation

of 533 m. From this station, the water is pumped to the "SHKABAJ" Water Treatment Plant via another DCI pipeline of the same diameter (DN 1200), rated for 16 bar (PN16) and extending approximately 4.5 km.

Throughout the pipeline system, there are more than 10 air valves, along with 7 sectional valves and 7 overflow valves. Notably, valve V1 serves as a sectional valve and is located near Node No. 28 at an elevation of approximately 590 m.

The entire water transmission process was monitored and analyzed using WHAMO software, which simulates hydraulic transients and water hammer effects within pressurized conduits. The analysis specifically focused on the main DN 1200 pipeline, approximately 14 km in total length. In the simulation, the pumps operated under normal conditions for the first 25 seconds. Subsequently, a transient event was introduced: the pumps were stopped after 25 seconds, and valve V1 was closed six seconds later.

Following pump shutdown at the inlet of the pumping station, the non-return valve closed automatically.

MATHEMATICAL MODEL OF WATER HAMMER

WHAMO is a computational tool developed by the Hydrologic Engineering Center (HEC) of the U.S. Army Corps of Engineers for simulating water hammer and mass oscillations in pressurized water conveyance systems [6]. The software is widely applied to evaluate the operational safety and dynamic behavior of hydraulic infrastructure such as pressure pipelines, tunnels, reservoirs, pumps, and turbines. The principal modelling capabilities of WHAMO can be summarized as follows:

- Hydraulic shock simulation: Calculates the pressure changes caused by stopping or starting pumps, closing valves, and changes in flow [8].
- *Transient analysis*: Simulates pressure waves and unsteady flows over time.
- Integration with other programs: Compatible with additional modeling platforms, such as HEC-RAS and other water system analysis tools, enabling comprehensive systemlevel evaluations [9].
- Numerical methods: Use differential equation techniques, such as characteristics and integration, to describe fluid movement.
- · Practical applications: Supports pipeline design and sizing, specification of surge protection devices, assessment of turbine and pump stability, and evaluation of hydraulic system resilience under transient loading [10].

Momentum Equation

Transient flow in closed conduits can be described using the fundamental continuity and momentum equations derived from the conservation of mass and Newton's second law of motion. Consider a one-dimensional flow in a pipe segment of constant diameter oriented along the x-axis, having a length Δx and a cross-sectional area A. The analysis of this control volume allows the derivation of the momentum equation through the equilibrium of pressure, inertial, and gravitational forces acting on the fluid element.

As shown in Figure 5, the flow direction is defined from left to right, with the dashed line representing the Hydraulic Grade Line (HGL), which indicates the actual energy distribution along the pipeline. It illustrates the moment when a pressure (shock) wave travels in the opposite direction of the primary flow as a result of a sudden disturbance, such as pump shutdown or valve closure.

These wave propagation phenomena are fundamental to the study of hydraulic transients and form the basis for modeling unsteady flow conditions in pressurized pipe systems.

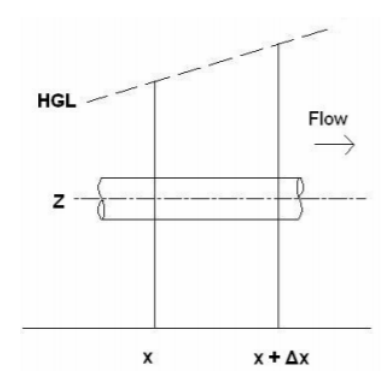


Figure 5. Tube with instant HGL [11].

At position x, the flow is Q and the piezometric head is H, which is the working pressure plus the static pressure (i.e. the pressure head plus the elevation head). At position $x + \Delta x$, the flow is $Q + \partial Q/\partial x \Delta x$ and the piezometric head is $H + \partial H/\partial x \Delta x$. Here, $\partial Q/\partial x$ and $\partial H/\partial x$ represent the partial derivatives of Q and H with respect to x, respectively, and are assumed to increase in the positive x direction. Figure 6 shows the forces acting on the fluid using a free-body diagram. The angle of the pipe is irrelevant for now, as the height of the pipe is accounted for in period H.

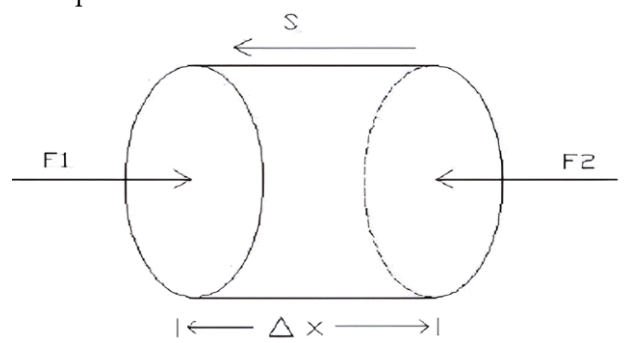


Figure 6. Free body diagram of a fluid element.

The full form of the equation (1) is as follows:

$$\frac{\partial V}{\partial t} + V \frac{\partial V}{\partial x} + \frac{1}{\rho} \frac{\partial p}{\partial x} + g \frac{\partial z}{\partial x} + \frac{f|V|V}{2D}$$
 (1)

This equation, together with the continuity equation that we will discuss below, is the basis for solving the water hammer problem in the WHAMO software.

Continuity Equation

As the water hammer pressure wave moves through a pipe, we want to analyze the following:

The elongation and expansion of the pipe wall due to the elasticity of the pipe wall and the compressibility of the fluid. Authors in [12] has derived the most general form of the control volume equation that considers both the motion and the deformation of the control volume. Based on the continuity equation for a moving control volume, the deformation control volume is written via equation (2) [13-17]:

$$\int_{C.V.} \frac{\partial \rho}{\partial t} dV + \int_{C.S.} \rho \overrightarrow{V_b} \overrightarrow{dA} + \int_{C.S.} \rho \overrightarrow{V_r} \overrightarrow{n} dA = 0$$
 (2)

Based on the hypotheses of [17, 18], the above equation in differential form is given by equation (3):

$$\frac{\partial H}{\partial t} + \frac{\partial Q}{\partial x} \frac{c^2}{gA} = 0 \tag{3}$$

Finite Difference Method

The momentum and continuity equations governing unsteady flow in pressurized conduits constitute a coupled system of hyperbolic partial differential equations for which no closed-form analytical solution is generally available. Consequently, several numerical techniques have been developed to solve the water hammer equations. The hyperbolic nature of the governing equations implies that their solutions propagate along welldefined characteristic paths. In the context of hydraulic transients, these paths correspond to the wave speed, which represents the defining characteristic of the system. This observation forms the basis of the Method of Characteristics (MOC), a widely used technique for solving hyperbolic systems. The MOC transforms the governing partial differential equations into a set of ordinary differential equations along characteristic lines, which can then be solved using explicit finite-difference schemes. A known limitation of the MOC is the requirement for sufficiently small-time steps to satisfy the Courant-Friedrichs-Lewy (CFL) stability condition, which may result in high computational effort for large systems or fine spatial discretization [14].

An alternative approach is the Finite Difference Method (FDM), in which the partial derivatives in the governing equations are replaced with finite-difference approximations. The implicit form of the method yields a system of algebraic equations that can be solved simultaneously at each time step. The primary advantage of the implicit finite difference approach is its enhanced numerical stability, allowing the use of relatively large time steps. However, for extensive hydraulic networks, this method requires solving a substantial number of nonlinear equations simultaneously, which increases computational complexity and solution time.

WHAMO software applies the implicit finite difference method, converting equations to a linear form for solution [15]. The solution space is discretized in the x-t plane, assigning specific values of H and Q at each grid point, H (x, t) and Q (x, t).

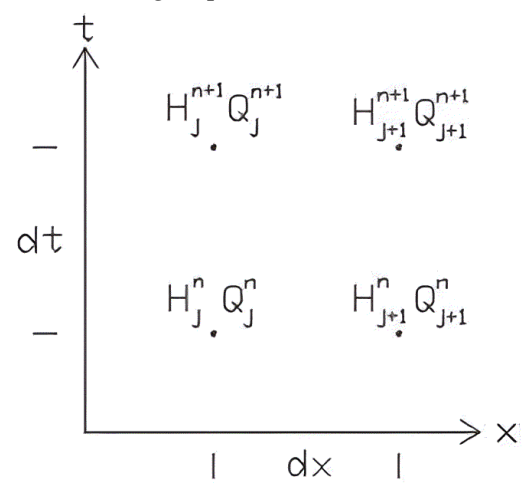


Figure 5. Finite Difference Network.

Some nodes in the solution network would represent a node in the system or a computational node within a pipe. The most common connection between two nodes in the computational network is a pipe, and the two equations of water hammer describe the relationships between energy and flow in the x- and t-directions. Other elements that connect nodes, such as valves and pumps, will be examined further.

To approximate the partial derivative with respect to time, take the average of the values of the function at the next time step, minus the average of the values at the current time step, all divided by the time step.

$$\frac{\partial H}{\partial t} = (H_{n+1,j+1} + H_{n+1,j} - H_{n,j+1} - H_{n,j})/(2\Delta t)$$
 (4)

And similarly, for the partial derivative of Q:

$$\frac{\partial Q}{\partial t} = (Q_{n+1,j+1} + Q_{n+1,j} - Q_{n,j+1} - Q_{n,j})/(2\Delta t)$$
 (5)

Approximation of partial derivatives with respect to the average of the next position step minus the average of the current position steps.

$$\frac{\partial H}{\partial x} = \frac{\theta}{\Delta x} \left(H_{n+1,j+1} - H_{n+1,j} \right) + \frac{(1-\theta)}{\Delta x} H_{n,j+1} - H_{n,j}$$
 (6)

and

$$\frac{\partial Q}{\partial t} = (Q_{n+1,j+1} + Q_{n+1,j} - Q_{n,j+1} - Q_{n,j})/(2\Delta t) \tag{7}$$

The two equations for the approximations of $\frac{\partial H}{\partial t}$ and $\frac{\partial Q}{\partial t}$ are as useful as those above, however, the variation method used by WHAMO includes an additional factor for calculating stability θ , and a value of 0.6 is used. With this additional factor, the equations become:

$$\frac{\partial H}{\partial x} = \frac{\theta}{\Delta x} \left(H_{n+1,j+1} - H_{n+1,j} \right) + \frac{(1-\theta)}{\Delta x} H_{n,j+1} - H_{n,j}$$
 (8)

and

$$\frac{\partial H}{\partial x} = \frac{\theta}{\Delta x} (Q_{n+1,j+1} - Q_{n+1,j}) + \frac{(1-\theta)}{\Delta x} Q_{n,j+1} - Q_{n,j})$$
(9)

Now, with the approximations for partial derivatives, we can substitute them into the momentum and continuity equations. After the substitution, the two equations are no longer differential equations but algebraic equations.

The momentum equation is as follows:

$$\frac{\Delta x_{j}}{2g\theta A_{j}} \left(Q_{n+1,j+1} + Q_{n+1,j} - Q_{n,j+1} - Q_{n,j} \right) + \left(H_{n+1,j+1} - H_{n+1,j} \right) + \frac{(1-\theta)}{\theta} \left(H_{n,j+1} - H_{n,j} \right) + \frac{\Delta x_{j} f_{j}}{4g\theta D_{j} A_{j}^{2}} \left(Q_{n,j} | Q_{n,j} | + Q_{n,j+1} | Q_{n,j+1} | \right) = 0$$
(10)

Where $Q \mid Q \mid$ is approximated $(Q_{n,j} \mid Q_{n,j} \mid + Q_{n,j+1} \mid Q_{n,j+1} \mid)/2$, thus linearizing the equation, greatly reducing the computational cost of solving it.

The continuity equation is as follows:

$$(H_{n+1,j+1} + H_{n+1,j} - H_{n,j+1} - H_{n,j}) + \frac{2\Delta t c_j^2 \theta}{g A_j \Delta x_j} (Q_{n+1,j+1} - Q_{n+1,j}) + \frac{2\Delta t c_j^2 (1-\theta)}{g A_j \Delta x_j} (Q_{n,j+1} - Q_{n,j}) = 0$$
(11)

These equations can be represented in a shorter form by introducing the following coefficients for the known values in a system. Using the same notation as the WHAMO program the coefficients are as follows:

$$\alpha_j = \frac{2\Delta t c_j^2 \theta}{g A_j \Delta x_j} \tag{12}$$

$$\beta_j = (H_{n,j+1} - H_{n,j}) + \frac{(1-\theta)}{\theta} \alpha_j (Q_{n,j} - Q_{n,j+1})$$
(13)

$$\gamma_j = \frac{\Delta x_j}{2g\theta A_j \Delta t} \tag{14}$$

$$\delta_{j} = \frac{(1-\theta)}{\theta} \left(H_{n,j} - H_{n,j+1} \right) - \frac{\Delta x_{j} f_{j}}{4g\theta D_{j} A_{j}^{2}} \left(Q_{n,j} \left| Q_{n,j} \right| + Q_{n,j+1} \left| Q_{n,j+1} \right| \right)$$
(15)

All parameters for the coefficient must be known from the properties of the pipe or from the values of pressure and flow in step with the elapsed time. With the coefficients, the momentum and continuity equations of the j^{th} pipe segment becomes⁶:

Moment:
$$-H_{n,j+1} + H_{n+1,j+1} + \gamma_j (Q_{n+1,j} + Q_{n+1,j+1}) = \delta_j$$
 (16)

Continuity:
$$H_{n,j+1} + H_{n+1,j+1} + \alpha_j (Q_{n+1,j+1} - Q_{n+1,j}) = \beta_j$$
 (17)

The initial conditions provide power and flow at the locations in the system. Now, there are four unknowns for the power and flow in the next step and two equations. This is why boundary conditions are needed. A boundary condition at each end of a branch is needed so that there are as many equations with unknowns as possible to solve the system [16]. There are three external boundary conditions that WHAMO uses the fixed reservoir pressure of the pumps, where $H_i = H_{\text{res-losses}}$, at the fixed flow where Qi = QBC, and the reservoir. There are internal boundary conditions, as well, at each node in the system. The energy equation and the continuity equation must be satisfied at each node. The node equations are as follows:

Power:
$$H_i = H_i - loss_{ii}$$
 (18)

$$H_i = H_k - loss_{ik} (19)$$

Continuity
$$Q_i + Q_j + Q_k = 0$$
 (20)

The energy equation states that the energy at node "i" is equal to that at node j minus the energy loss between the nodes. The continuity equation states that the sum of the flows into and out of a node is equal to zero. Other important features or elements in the system are small losses, valves, and pumps. The mathematics of representing a pump in the system is complicated.

Local losses in the pipe a are represented by the term $C_{add} \frac{|Q|Q}{2gA^{2\prime}}$ and are simply added to the loss formulas in the momentum equation, where C_{add} is the small loss coefficient. The total head loss term in the momentum equation is:

$$\left(\frac{\Delta x_{j} f_{j} + C_{add}}{4g\theta D_{j} A_{j}^{2}}\right) \cdot \left(Q_{n,j} |Q_{n,j}| + Q_{n,j+1} |Q_{n,j+1}|\right)$$
(21)

For a valve, the flow is based on the formula:

$$Q = C_q D^2 \sqrt{g} \Delta H \tag{22}$$

Rearranging the formula to the form after the substitutions we have:

$$H_{n+1,j} - H_{n+1,j+1} = -\frac{1}{C_n^2 D^4 g} Q_{n+1,j} |Q_{n+1,j}|$$
 (23)

The notation $Q_{n+1,j} | Q_{n+1,j} |$ is used instead of $Q_{n+1,j}$ to allow for sign change. Linearizing the equation then becomes:

$$H_{n+1,j} - H_{n+1,j+1} = \frac{2|Q_{n,j}|}{C_q^2 D^4 g} Q_{n+1,j} - \frac{1}{C_q^2 D^4 g} Q_{n,j} |Q_{n,j}|$$
(24)

The continuity equation for valves is simple: the flow on one side of the valve is equal to the flow on the opposite side of the valve [17].

$$Q_{i+1} = Q_i \tag{25}$$

The discharge coefficient, Cq, can be related to the pressure loss coefficient by the following expression:

$$C_q = \frac{\pi}{\sqrt{8}\sqrt{C_h}} \tag{26}$$

and

$$C_h = \frac{\Delta h}{V^2/2g} \tag{27}$$

Now, using the equations for all the connections and nodes in the system, the initial and boundary conditions, a matrix of a linear system of equations can be constructed that will solve for pressure and flow simultaneously for the first time. The procedure is repeated for the next step and again for the next step, until the specified end of the simulation [19].

Various real physical characteristics are converted into mathematical modeling blocks, and then the system is assembled and simulated in different scenarios using the WHAMO computer program [20].

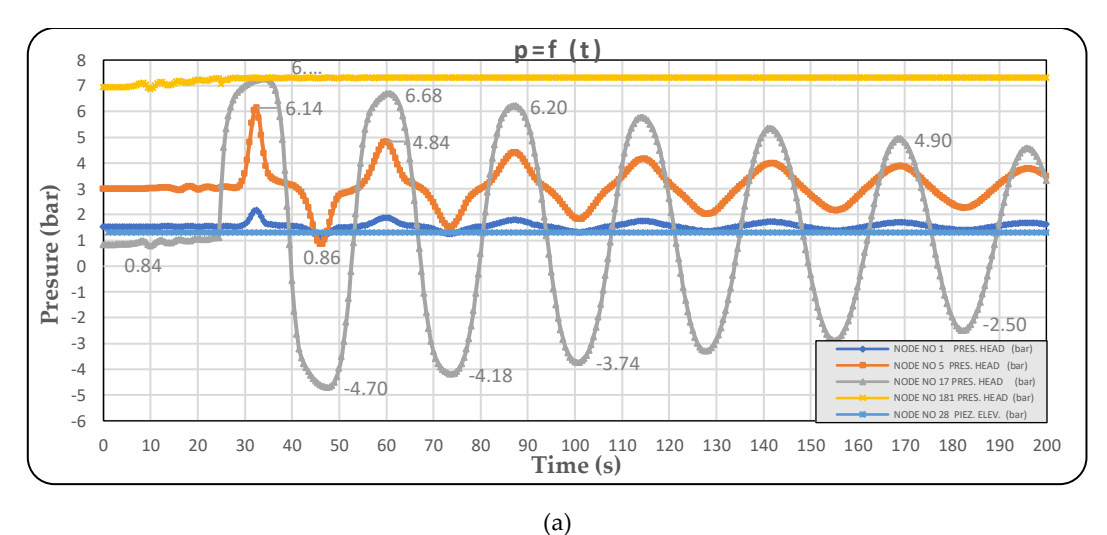
Table 4 depicts all the data for nodes in the main pipe.

Table 4. Data for nodes in the main pipe

SIMU	HISTOR	SIMULATION - OUTPUT TIME HISTORIES FOR RU	SIMULATION - OUTPUT TIME HISTORIES FOR RUN OF 10/14/19 AT		10:44:46				TITLED	: PUMPIN	G STATIC	JN - PRIS	TITLED: PUMPING STATION - PRISHTINA n=1320 rpm	1320 rpm	
Time	Node no.	1 Node no.	Time Node no. 1Node no. Node no. 1 Node no. 5Node no.	Node no. 5	Node no.	Node no 5	Node no 17Node noNode no 17	Node no	Node no 17	Node	Node no	Node no	Node no Node no Node no 28 Node no Node no 28	Node no	Node no 28
(s)	static	1 flow	Potential	static	гv	Potential	static	17	Potential	no.181	181 flows	181	static	28 flows	28 flows Potential
	pressure	(1/s)	energy	pressure	flow	energy	pressures	flow	energy	static	(1/s)	Potential	pressures	(I/s)	energy
	(bar)		(m)	(bar)	(1/s)	(m)	(bar)	(1/s)	(m)	pressure (bar)		energy (m)	(bar)		(m)
0	1.54	614.48	544.46	3.00	614.48	544.13	0.84	614.48	541.66	6.94	614.48	605.33	1.30	614.48	599.79
0.5	1.54	614.48	544.46	3.00	614.48	544.13	0.84	614.48	541.66	6.94	614.48	605.33	1.30	614.48	599.79
1	1.54	614.48	544.46	3.00	614.48	544.13	0.84	614.48	541.66	6.94	614.48	605.33	1.30	608.81	599.79
1.5	1.54	614.48	544.46	3.00	614.48	544.13	0.84	614.48	541.66	6.94	614.48	605.33	1.30	597.49	599.79
2	1.54	614.48	544.46	3.00	614.48	544.13	0.84	614.48	541.66	6.94	614.48	605.33	1.30	583.33	599.79
2.5	1.54	614.48	544.46	3.00	614.48	544.13	0.84	614.48	541.66	6.94	614.48	605.33	1.30	563.51	599.79
3	1.54	614.48	544.46	3.00	614.48	544.13	0.85	614.48	541.66	6.94	614.48	605.33	1.30	538.02	599.79
3.5	1.54	614.48	544.46	3.00	614.48	544.13	0.85	614.48	541.66	6.94	614.48	605.36	1.30	504.04	599.79
4	1.54	614.48	544.46	3.00	614.48	544.13	0.85	614.48	541.69	6.94	614.48	605.39	1.30	441.74	599.79
4.5	1.54	614.48	544.46	3.00	614.48	544.13	0.85	614.48	541.72	6.95	614.48	605.42	1.30	336.97	599.79
Ŋ	1.54	614.48	544.46	3.00	614.48	544.13	98.0	614.48	541.78	96.9	614.48	605.52	1.30	220.87	599.79
5.5	1.54	614.48	544.46	3.00	614.48	544.13	98.0	614.48	541.84	96.9	614.48	605.61	1.30	87.78	599.79
9	1.54	614.48	544.46	3.00	614.48	544.13	0.87	611.64	541.96	86.9	611.64	605.73	1.30	11.33	599.79
6.5	1.54	614.48	544.46	3.00	614.48	544.13	0.89	611.64	542.09	6.99	611.64	88.509	1.30	-14.16	599.79
^	1.54	614.48	544.46	3.00	614.48	544.13	0.91	608.81	542.30	7.02	608.81	606.16	1.30	-14.16	599.79
7.5	1.54	614.48	544.46	3.00	614.48	544.13	0.94	86:209	542.57	2.06	86.509	606.55	1.30	-5.66	599.79
8	1.54	614.48	544.46	3.00	614.48	544.13	0.97	603.15	542.91	7.10	603.15	606.95	1.30	-2.83	599.79
8.5	1.54	614.48	544.46	3.00	614.48	544.16	0.98	603.15	543.03	7.11	603.15	607.10	1.30	0.00	599.79
6	1.54	614.48	544.46	3.00	614.48	544.16	0.93	608.81	542.51	7.05	608.81	606.40	1.30	0.00	599.79
9.5	1.54	614.48	544.46	3.01	614.48	544.16	0.83	617.31	541.51	6.91	617.31	602:09	1.30	0.00	599.79
10	1.54	614.48	544.46	3.01	614.48	544.19	0.78	620.14	541.02	98.9	620.14	604.54	1.30	0.00	599.79
10.5	1.54	614.48	544.46	3.01	614.48	544.22	0.83	617.31	541.54	6.93	617.31	605.21	1.30	0.00	599.79
11	1.54	614.48	544.49	3.02	614.48	544.28	0.90	611.64	542.24	7.02	608.81	60.909	1.30	0.00	599.79
11.5	1.54	614.48	544.49	3.02	611.64	544.34	96.0	86:209	542.82	7.09	86.509	98.909	1.30	0.00	599.79
12	1.54	611.64	544.49	3.03	611.64	544.43	1.01	600.32	543.31	7.15	600.32	607.47	1.30	0.00	599.79
12.5	1.54	611.64	544.53	3.04	608.81	544.53	1.00	600.32	543.25	7.14	600.32	607.34	1.30	0.00	599.79
13	1.54	608.81	544.56	3.05	608.81	544.62	0.95	86:209	542.73	7.07	86:509	29.909	1.30	0.00	599.79
199.5	1.64	-223.70	545.50	3.55	-218.04	549.74	3.60	0.00	569.64	7.31	0.00	609.02	1.30	0.00	599.79
200	1.63	-249.19	545.35	3.49	-243.52	549.07	3.31	0.00	566.71	7.31	0.00	609.02	1.30	0.00	599.79

The Outcomes of the Work

Figure 6 depict the water flow comparison at selected nodes in the main pipe by using an expansion vessel.



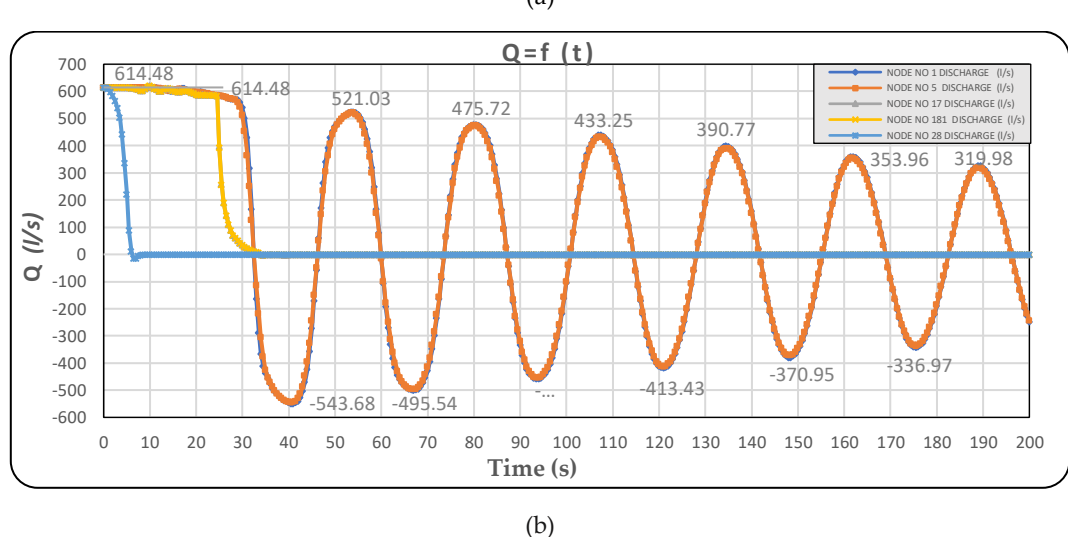


Figure 6. Water flow comparison at selected nodes in the main pipe, using an expansion vessel. Pump speed is set to n=1320 rpm, total flow rate is Q_{tot}=700 l/s, and valve V1 is closed. (a)- Water pressure in the joint p (bar), (b)- Water flows at node Q (l/s)

In this simulation, the pressure at the inlet of the pump station is 0.84 bar, and at the outlet of the pump station is 6.94 bar, while the pump flow is 614.48 l/s. The pump operates at a speed of 1320 rpm. The power of the pump's electric motor consumes 265.02 kW of energy while it is operating. We close the V1 Valve at second 6 and the pumps continue to operate until second 25. The pumps are switched off at 25 seconds, and we have the following situation.

The most critical point in the system occurs at node 17, where a pressure change of 1.3 bar is observed at second 25, accompanied by a flow of 614.48 l/s. This is caused by a wave

traveling in the opposite direction, which subsequently generates a reverse pressure of -4.7 bar at second 40, along with a reverse flow of -543.68 l/s.

These oscillations continue over time. At second 55, the system records a flow of 521.03 and a pressure of 6.68 bar. At second 67.5, the flow reversed to -495.54 l/s, followed by a pressure of -4.09 bar at second 72.5. The pressure and flow values at node 17 continue to decrease thereafter, as illustrated in Figure 6a.

The risk of cavitation is present until the second 100, because we have the pressure - 3.74 bar and the flow is -450.29 l/s, the system does not calm down even after the second 200.

This situation is very dangerous, and here, the possibility of cavitation is very high, and with it, the destruction of the pipe at this junction is possible.

The WHAMO software does not consider the change of phases, so the simulation with the WHAMO software produces opposite pressures that exceed the vapor pressure, and the software only warns of the possibility of the occurrence of the cavitation phenomenon, and with it, the possibility of the destruction of the water pipe.

Regarding the flow at these nodes, the following situation occurs at node 28, where the valve of the closed sector is located: we have a flow, but not after this time, i.e., after 6 seconds. While at node 181, we have a flow of 583.33 l/s until the pumps start working at second 25. After this moment, we have a decrease in flow until second 34 when the flow drops to 0 l/s. The situation is the same at node no. 17, which can also be seen in Figure 6b and in Table 5 [7].

Table 5. Maximum and minimum static pressure and maximum and minimum flow rates of pumps

Name	Stationing (m)		Maximum lift energy		Minimum lift-off	Time (s)	Maximum flow	Time (s)	Minimum Flow	Time (s)
		(m)	(m)		energy (m)		(1/s)		(1/s)	
Node 0	0	544.53	544.53	0	544.53	0	614.48	0	-549.35	41
Node 1	203.5	528.79	550.99	32.5	540.26	46	614.48	0	-549.35	41
Node 2	367.35	528.67	556.08	32.5	536.84	46	614.48	0	-549.35	41
Node 3	499.17	518.17	560.04	32.5	534.13	46	614.48	0	-549.35	41
Node 4	1054.83	516.60	574.79	32.5	523.22	46	614.48	0	-546.52	40.5
Node 5	1114.93	513.50	576.13	32.5	522.12	46	614.48	0	-546.52	40.5
Node 6	1504.4	518.45	583.60	32.5	515.33	46	614.48	0	-543.68	40.5
Node 7	1582.57	513.96	584.85	32.5	514.05	46	614.48	0	-543.68	40.5
Node 8	2651.79	522.95	595.67	32	500.27	46	614.48	0	-529.53	40
Node 9	3664.09	532.03	600.46	32.5	493.11	46	614.48	0	-512.53	39.5
Node 10	4387.55	533.61	602.38	33	490.36	46	617.31	13.5	-492.71	39
Node 11	4577.23	534.74	602.83	33	489.84	46	617.31	13.5	-489.88	39
Node 12	4634.47	530.45	602.96	33	489.69	46	617.31	13	-487.05	39
Node 13	4700.19	535.25	603.08	33	489.54	46	617.31	13	-484.22	39
Node 14	5238.22	522.87	604.14	33.5	488.35	46.5	617.31	12.5	-464.40	39

Node 15	6964.55	528.31	606.22	34	485.70	47	617.31	11.5	-283.17	39.5
Node 16	7591.42	533.57	606.80	34.5	485.18	47.5	620.14	10.5	-167.07	39.5
Node 17	8359.53	532.97	607.44	34.5	484.97	47.5	620.14	10	-2.83	34.5
Node 18	8980	534.54	609.14	35	604.54	10	311.49	10	-2.83	34.5
Node 181	9531.16	535.90	609.14	28	604.54	10	620.14	10	-2.83	34.5
Node 182	9531.16	535.90	609.08	32	605.06	10	858.00	9	-16.99	34.5
Node 19	10082.32	537.34	642.37	8	582.20	10	614.48	0	-8.50	8
Node 191	10087.32	540.69	675.56	9.5	605.03	0	614.48	0	-8.50	8
Node 20	10734.65	545.12	673.18	10	604.81	0	614.48	0	-118.93	8.5
Node 21	11613.12	580.61	673.18	8	604.48	0	614.48	0	-93.45	9
Node 22	12284.78	566.19	668.67	7.5	604.48	0	614.48	0	-59.47	9.5
Node 23	12417.31	568.66	672.39	7	604.33	0	614.48	0	-53.80	9.5
Node 24	12676.37	564.37	672.79	7	604.27	0	614.48	0	-39.64	9.5
Node 25	12877.59	570.80	673.58	7	604.17	0	614.48	0	-25.49	9.5
Node 26	12971.74	566.80	673.61	12.5	604.11	0	614.48	0	-16.99	9.5
Node 27	13225.01	586.58	674.07	12.5	604.08	0	614.48	0	-14.16	6.5
Node 28	13465.05	599.79	674.67	0	604.02	0	614.48	0	-14.16	6.5

Node number 5 is identified as the most critical node. Additionally, we observe significant fluctuations in water flow, ranging from 614.48 l/s at the 30th second to -543.68 l/s at the 40th second. These flow variations, characterized by oscillations, persist as illustrated in Figure 6b and do not stabilize even after 200 seconds, although the intensity of the flows gradually diminishes.

Table 6 depict the power of electric motors with maximum and minimum flow rates of pumps.

Table 6. Power of electric motors with maximum and minimum flow rates of pumps

Time (s)	No. of rotations of	Pump motor	Pump flow P ₁	No. of rotations	Pump motor	Pomp Flow P2	Expansion Vessel	Opening the Valve	
(=)	the pump P ₁ (rpm)			of the pump P ₂	power P ₂ (kW)		Flows (1/s)	V ₁ (%)	V ₁ (1/s)
	•			(rpm)					
0	1320	0.00	308.65	1320	0.00	308.65	0.00	100	614.48
0.5	1320	265.02	308.65	1320	265.02	308.65	0.00	92.5	608.81
1	1320	265.02	308.65	1320	265.02	308.65	0.00	80	597.49
1.5	1320	265.02	308.65	1320	265.02	308.65	0.00	70	583.33
2	1320	265.02	308.65	1320	265.02	308.65	0.00	60	563.51
2.5	1320	265.02	308.65	1320	265.02	308.65	0.00	50	538.02
3	1320	265.02	308.65	1320	265.02	308.65	0.00	40	504.04
3.5	1320	264.95	308.65	1320	264.95	308.65	2.83	29.4	441.74
4	1320	264.95	308.65	1320	264.95	308.65	8.50	20	336.97
4.5	1320	264.80	308.65	1320	264.80	308.65	19.82	14.4	220.87
5	1320	264.72	305.82	1320	264.72	305.82	39.64	10	87.78
5.5	1320	264.57	305.82	1320	264.57	305.82	70.79	3.8	11.33
6	1320	264.35	305.82	1320	264.35	305.82	113.27	0	-14.16
6.5	1320	264.05	305.82	1320	264.05	305.82	172.73	0	-14.16
7	1320	263.60	305.82	1320	263.60	305.82	260.51	0	-5.66
7.5	1320	263.01	302.99	1320	263.01	302.99	385.11	0	-2.83

8	1320	262.26	302.99	1320	262.26	302.99	555.01	0	0.00
8.5	1320	262.04	300.16	1320	262.04	300.16	739.07	0	0.00
9	1320	263.16	302.99	1320	263.16	302.99	858.00	0	0.00
9.5	1320	265.39	308.65	1320	265.39	308.65	812.69	0	0.00
10	1320	266.36	311.49	1320	266.36	311.49	637.13	0	0.00
10.5	1320	265.25	308.65	1320	265.25	308.65	478.55	0	0.00
11	1320	263.75	305.82	1320	263.75	305.82	421.92	0	0.00
11.5	1320	262.49	302.99	1320	262.49	302.99	461.56	0	0.00
12	1320	261.44	300.16	1320	261.44	300.16	580.50	0	0.00
12.5	1320	261.59	300.16	1320	261.59	300.16	707.92	0	0.00
13	1320	262.78	302.99	1320	262.78	302.99	758.89	0	0.00
200	0	0.00	0.00	0	0.00	0.00	0.00	0	0.00

The static pressure measurements at the study nodes reveal some notable trends. Pressure was recorded at 544.31 m on the 25th second, increasing to 606.58 m by the 35th second before decreasing to 485.09 m at the 45th second. This oscillatory pattern continues, as illustrated in Figure 7. These oscillations suggest a moderate level of risk to the water transport system at node 17. In contrast, other nodes display a low level of risk as they do not experience significant oscillations. The large oscillations at node 17 are primarily caused by the V1 valve closing at the 6th second. Furthermore, pressure fluctuations at this node are also due to the movement of a large volume of water in the DN 1200 main pipe [12].

Potential energy values H (m)

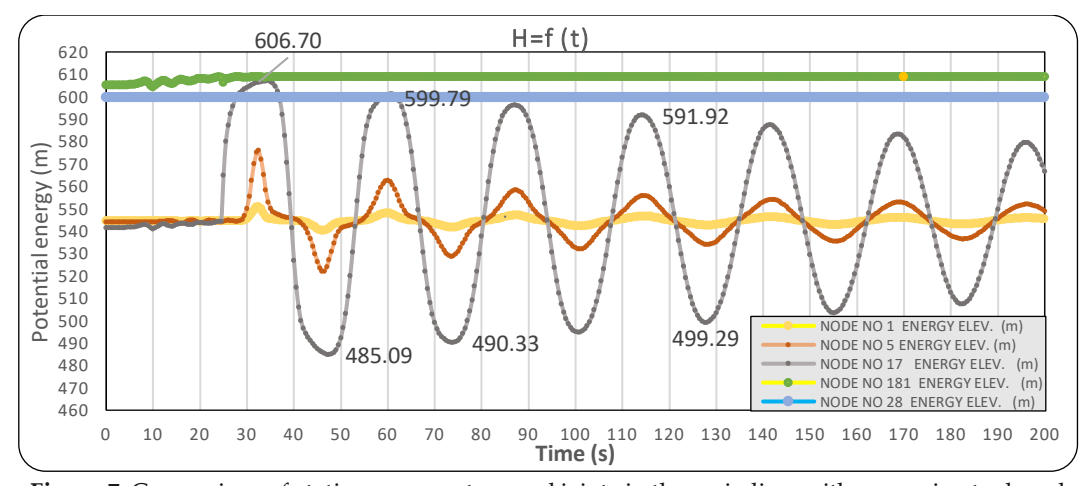


Figure 7. Comparison of static pressure at several joints in the main line, with expansion tank and pump speed n=1320 rpm, Qtot=700 l/s, V1 closing.

In this simulation, the inlet pressure at the pump station is 0.84 bar and the outlet pressure is 6.94 bar, with a pump flow of 614.48 l/s. The pump operates at a speed of 1320 rpm. The power of the pump's electric motor consumes 265.02 kW of energy while it is operating. We close the V1 Valve at second 6 and the pumps continue to operate until second 25. The pumps are switched off at 25, and we have the following situation.

Node 17 is the most critical point in the system. At the 25-second mark, there is a pressure change of 1.3 bar and a flow rate of 614.48 l. A reverse pressure of -4.7 bar is

generated by a wave travelling in the opposite direction at second 40, with a flow of -543.68 l/s against the flow.

Afterward, at second 55, we have a flow of 521.03 l/s and a pressure of 6.68 bar. At second 67.5, the flow is -495.54 l/s and the pressure is -4.09 bar. This continues. The pressure and flow continue to decrease at node no. 17, as shown in Figure 6b.

The risk of cavitation remains until second 100, when the pressure is -3.74 bar and the flow is -450.29 l/s. Even after second 200, the system does not calm down.

This situation is extremely dangerous, with a high risk of cavitation and pipe destruction at this junction.

The WHAMO software does not handle phase changes, so simulations using WHAMO produce opposite pressures that exceed the vapor pressure. The software only warns of the possibility of cavitation and pipe destruction. Figure 8 depict the Comparison of the percentage of opening V1 during 6s, and the amount of water entering the expansion vessel.

V1 % =f (t) 100 ELEMENT V1 GATE OPENING (%) 950 90 858.00 850 ELEMENT TANK DISCHARGE (I/ 80 758.89 750 690.93 70 650 614.48 ≈ ⁶⁰ 550 50 450 484.22 40 421.92 350 30 250 20 150 113.27 0.00 10 50 -50 10 12 14 16 18 20 22 24 26 28 30 32 34 36 38 40 42 44 Time (s)

Pump flow Q=f(t) and valve position $A_v = f(\%)$

Figure 8. Comparison of the percentage of opening V1 during 6s, and the amount of water entering the expansion vessel

In the Figure 8, the closing of valve V1 over a period of 6 seconds is illustrated with a full red curve, representing the percentage of the valve closing. The full blue curve shows the flow through valve V1 as a function of time, while the full black curve depicts the flow in the expansion vessel. As observed in Figure 5, until the 6th second when valve V1 closes—the expansion vessel experiences a water flow of 113.27 l/s. At the 9-second mark, the flow in the expansion vessel increases to 858 l/s, followed by an oscillation where the flow drops to 421.92 l/s. This flow continues until the 25-second mark, then at 27.5 seconds, it decreases to 62.30 l/s, ultimately dropping to 0 l/s by the 50-second mark.

In the Figure 9, the water flow through Valve V1 is time-dependent, and we have included the percentage of Valve V1's opening over a duration of 6 seconds.

% = f(t), Q=f(t)100 650 ELEMENT V1 GATE OPENING (%) 597.49 90 563.51 614.48 ELEMENT V1 GATE DISCHARGE (1/s) 550 80 504.04 70 450 60 350 336.97 50 40 250 30 87.78 0.00 150 20 10 50 0 -14.16 -50 -10 0 5 10 Time (s)

Comparison between Q and %

Figure 9. Comparison of the percentage of opening V1 for 6s, and the water flow through Vale V1.

It is noteworthy that, up until the 6th second, the valve remains open at the percentages indicated in the following table 7.

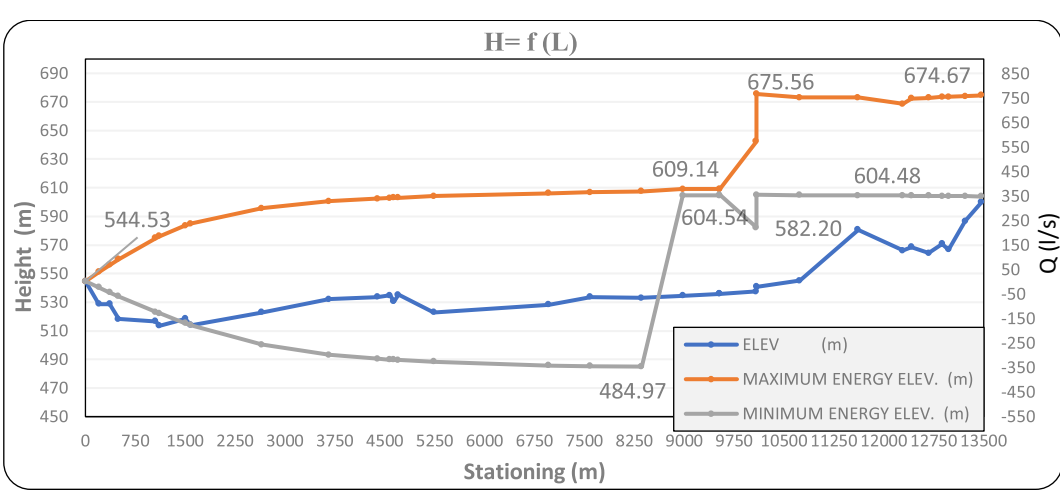
	14010 / 110	10011111190 01	· carve · r s o _l			o occorion.	
Time (s)	.00	1.00	2.00	3.00	4.00	5.00	6.00
Percent (%)	100	80	60	40	20	10	.00

Table 7. Percentage of Valve V1's opening over a duration of 6 seconds

At second 0, the valve is fully open at 100%, allowing 614.48 l/s of unobstructed water flow. At second 1, the valve is open to 80%, resulting in a flow of 600 l/s. At second 2, the valve opening has decreased to 60%, and the water flow through valve V1 is 563.51 l/s. The valve continues to close, and at Second 3 its opening is 40%, with a corresponding flow of 504.04 l/s. At second 4, the valve is now only 20% resulting in a flow of 336.97 l/s through V1. At second 5, the valve is reduced to 10% open, and the water flow through valve V1 has dropped to 87.78 l/s. Finally, at second 6, the valve is completely closed, resulting in an implied negative flow of -14.16 l/s.

Figure 10 shows the steady state condition when two pumps operate at a speed of n = 1320 rpm with a total flow in the pipeline Q_{tot} = 614.48 l/s. Thus, the blue line (solid) represents the potential energy of the position (i.e. the height of the pipeline – m.a.s.l) at the nodes along the length of the pipeline that we have selected for study (supply pipe nodes 1, 5, 17 and pressure pipe nodes 181, 28). In Figure 7, the red pipeline line (solid) represents the total potential energy at the nodes along the length of a pipeline with a steady state operation of two pumps.

From this curve, the change in static pressure at each point of the pipeline can be read.



Comparison between max. potential energy and min. potential energy

Figure 10. Comparison of pressure at several joints in the main pipe, with expansion vessel and pump speed n=1320 rpm.

CONCLUSION

This research work provides a comprehensive assessment of the hydraulic performance, operational efficiency, and technical characteristics of the DN 1200 water transmission pipeline, which forms an integral part of the regional supply system serving Prishtina, Obiliq, Fushe Kosove, and several surrounding municipalities. The system includes the main pipeline, the pump stations (nodes 17 and 181), and the water treatment plant (node 28), all functioning together to ensure the reliable delivery of drinking water to the region.

The transmission pipeline is constructed from cast iron pipes in accordance with the DIN EN 545 standard, protected externally with zinc-aluminum and bitumen coatings and internally lined with cement mortar. The hydraulic roughness values considered for the analysis were [21]:

- k = 0.85 (average for cement-lined cast iron),
- k = 1.15 (maximum for cement-lined cast iron), and
- k = 3.00 (representative of corrosion conditions).

According to the manufacturer, the use of these pipe materials yields several significant advantages, including reduced raw water intake, lower hydraulic losses, minimized staffing needs at pumping facilities, decreased risk of physical damage, and reduced environmental impact.

A comparison between the measured pump flow rates and the design performance test results revealed a decline in pump efficiency from the expected 86% to 61.8% in operation [22]. This reduction has a direct impact on energy consumption, resulting in higher operating costs for delivering the same quantity of water. Calculations indicate that a single pump operating under optimal conditions could save approximately 727,605.6 kWh annually. At an electricity cost of €0.08/kWh, this translates into an annual saving of

€58,208.44 per pump. Given that two pumps typically operate simultaneously, the potential savings could reach €116,416.89 per year.

The hydraulic analysis also highlights the importance of preventing pump dry running [23, 24]. When water losses exceed 300 l/s, the pipeline cannot sustain flows above 1,250 l/s, potentially endangering pump operation. Installing a dry-running protection system would provide immediate shutdown under unsafe conditions and significantly reduce the risk of mechanical damage.

Based on the outcomes of this research work, the following actions are recommended for the Regional Water Supply Company "PRISHTINA" to minimize unnecessary operational costs and enhance system reliability:

- Replacement of inefficient pumps;
- Correction of errors in pump selection and sizing;
- Impeller trimming or other performance-optimizing interventions.

These measures represent both technically sound and economically justified solutions, and it is anticipated that, within a three-year period, investments in new pumping equipment or improvements to existing units would generate substantial financial and operational benefits for the utility.

NOMENCLATURE

```
H – hydraulic head,
J – spatial index (pipe node),
N – time step duration,
H_{n,j}-head at time step n, node j,
H_{n+1,j}-head at time step n+1, node j,
Q – flow rate (discharge) in the pipe,
t- time,
\partial Q/\partial t – Partial derivative of Qwith respect to time (rate of change of Qin time),
n- time step index,
j – spatial index (an integer identifying the position in space on the numerical grid),
Q_{n,i} - value of Q at time step n and spatial index j,
Q_{n+1,j} -value of Q at the next time level n+1 at the same spatial position j,
Q_{n,j+1}-value of Q at the same time n, but at the next spatial location j+1,
Q_{n+1,j+1} – Value of Q at the next time step and the next spatial position,
\Delta t– Time step size (the difference between time levels t_{n+1} and t_n),
Q(n,j) - flow rate at time step n and node j,
Q(n, j + 1) - flow rate at time step n and the next spatial node j+1,
|Q| - absolute value of flow rate (express flow-dependent friction terms),
\Delta xj - pipe segment length between nodes j and j+1,
```

fj - Darcy–Weisbach friction factor for the pipe segment, θ (*theta*) -angle factor or correction term (often 1 for horizontal pipes,

AUTHOR CONTRIBUTIONS

Conceptualization, Gj.V. and Z.S.; Methodology, Gj.V.; Validation, M.I., Z.S. and E.V.; Investigation, Gj.V.; Resources, Gj.V.; Data Curation, Gj.V.; Writing – Original Draft Preparation, Z.S.; Writing – Review & Editing, Gj.V.; Visualization, E.V.; Supervision, Z.S.; Project Administration, E.V.

CONFLICT OF INTERESTS

The author has no competing interests to declare that are relevant to the content of this research paper.

REFERENCES

- 1. Lupa, S-I., Gagnon, M., Muntean, S., Abdul-Nour, G. The Impact of Water Hammer on Hydraulic Power Units. *Energies.* **2022**, 15(4), 1526
- 2. Afshar, M. H. & Rohani, M. Water hammer simulation by implicit method of characteristic. *International Journal of Pressure Vessels and Piping.* **2008**, 85, 851–859.
- 3. Kren, J., Tiselj, I. & Division, R. E. Exploring Taylor Bubble Dynamics in Counter-Current Flows: A Combined Numerical and Experimental Study. 33d International Conference Nuclear Energy for New Europe. Portoroz, Slovemia, 9-12 September. 2024, p. 1–8.
- 4. Anderson, J. D. Governing Equations of Fluid Dynamics. 2009.
- Butcher, C. Damage-Based Fracture Modelling of Mild And Advanced High Strength Steel. Available from: https://www.steel.org/wp-content/uploads/2024/06/11.30-T3_C-Butcher_Damage-Based-Fracture-Modelling.pdf (Access date: 20 August 2025).
- Lohrasbi, A.R., Attarnejad, R. & Member, F. Water Hammer Analysis by Characteristic Method. American J. of Engineering and Applied Sciences, 2008, 1(4), 287–294.
- 7. Vataj, G., Ismayilov, M., & Sejfijaj, Z. Energy Generation from Water Systems: A Technical and Cost-Benefit Analysis. International Journal of Innovative Technology and Interdisciplinary Sciences, 2025, 8(3), 537–549.
- 8. Constantin, A. & Nitescu, C. S. Numerical Simulation of Hydraulic Shock in a Water Pumping System Protected by Air 2 Pumping Installation Protection from Water Hammer 3 Case Study. *WSEAS Transctions on Systems*, **2010**, 9(10), 1009–1018.
- 9. HEC-RAS User 's Manual. Available from: https://www.hec.usace.army.mil/software/hec-ras/documentation/HEC-RAS%20User's%20Manual-v6.4.1.pdf (Access date: 20 August 2025).
- 10. Itissam, A., Oulhaj, A., Sebari, K. & Ouazar, D. Sizing the Protection Devices to Control Water Hammer Damage. *Int. J. Civil, Archit. Sci. Eng.* **2013**, *7*, 415–420.
- 11. Drainage, S. Storm Drainage 13-G-1. Available from: https://up.codes/viewer/florida/fl-plumbing-code-2014/chapter/11/storm-drainage#11 (Access date: 20 August 2025).
- 12. Covas, D., Técnico, I. S. & Pais, A. R. The dynamic effect of pipe-wall viscoelasticity in hydraulic

- transients . Part II model development , calibration and verification L $^\prime$ effet dynamique de la viscoélasticité de la conduite en régimes transitoires hydrauliques . Partie II développement **2005**, 43, 56–70.
- 13. Bansal, R.K. A Textbook of Fluid Mechanics and Hydraulic Machines. Availbe from: https://books.google.lk/books?id=0clZbfwgiyUC&printsec=copyright#v=onepage&q&f=false (Access date: 20 August 2025).
- 14. Tsogtgerel, G. Method of characteristics and the Courant-Friedrichs-Lewy condition Characteristic curves. Available from: https://www.math.mcgill.ca/gantumur/math319w11/downloads/slides12.pdf. (Access date: 20 August 2025).
- 15. Ali, N. A., Abozeid, G. & Darweesh, M. S. Analysis Of Different Protection Methods Against Water Hammer On Water Supply Network (Case Study-Assiut City Network). *JES. Journal of Engineering Science*, **2013**, 41(6) 2021–2035.
- 16. Tijsseling, A. S. & Vardy, A. E. Some Intriguing Aspects Of Boundary Conditions In Water Hammer. 37th IAHR World Congress, Kuala Lumpur, Malasya, 13-18 August, **2017**, p. 4-7.
- 17. Mukilan, S., Vivek, E. A Review On Continuity Equation For One And Three. *Industrial Engineering Journal*, **2023**, 52(4), 115-119.
- 18. Street, R., Watters, G., and Vennard, J. Elementary Fluid Mechanics. 7th Edition, John Wiley & Sons, New York. 1996.
- 19. Todini, E. & Ferrante, M. Matrix formulation of steady / unsteady-state models in complex pressurized pipe systems. **2018**, *3*, 2081–2087.
- Ghidaoui, M.S., Zhaoi, M., Mcinnis, D.A., & Axworthy, D.H. A Review of Water Hammer Theory and Practice. Applied Mechanics Review, 2005, 58, 49–76.
- 21. Ductile Iron Pipes and Fittings. Available from: https://www.kembla.com.hk/images/Ductile%20Iron%20Pipe%20&%20fittings%20BSEN%2054 5%20&%20BSEN%20598.pdf (Access date: 10 August 2025).
- 22. Menon, S. Centrifugal Pump Analysis. 2012, p. 1-69.
- 23. Pandey, K., Deepak, G., Monil, D. & Prateek, H. S. Pump Dry Run Prevention System. Int. J. Sci. Res. Dev. 2016, 4, 1947–1951.
- 24. Abou EL-Hassan, azza., Khairat Dawood, M. M., EL Morse, M. S., Abdel-Mageed, S. I., & A. Sharaf, O. The Effective Techniques for Enhancing the Turbulent Flow Between Two Parallel Plates: A Comprehensive Review. *Journal of Transactions in Systems Engineering*, 2023, 1(1), 10–30.